Strojniški vestnik - Journal of Mechanical Engineering 70(2024)7-8, 369-380
DOI:10.5545/sv-jme.2023.902
Original Scientific Paper
Received for review: 2023-12-20
Received revised form: 2024-04-22
Accepted for publication: 2024-06-19

Dynamic and Phase-Frequency Characteristics of Rotor Instability Induced by Steam Flow Excited Vibration in Seals

Dacai Li [1,*] – Changhong Lv [1] – Zhenhai Bu [1] – Xuming Yan [1] – Zili Lan [1] – Lihua Cao [2] – Heyong Si [2]
[1] Guangdong Datang International Leizhou Power Generation Co., Ltd., China
[2] Northeast Electric Power University, School of Energy and Power Engineering, China

Steam flow excited vibration in seals seriously affects the seal-rotor stability. A mesh deformation based on user-defined functions was adopted to establish the multi-frequency whirl model, and the reliability of the simulation method was verified by experiments. The average effective damping and working ability of the fluid were proposed to analyse the stability of the seal. The mechanism of seal instability induced by steam flow excited vibration was revealed through the phase-frequency characteristics of exciting forces and displacements. The results show that direct damping decreases gradually with an increase in frequency, and the cross-coupling damping tends to be stable over 15 Hz. The average effective damping is more sensitive and accurate in predicting the seal stability. Effective damping decreases with increased frequency. Therefore, the rotor stability is decreased. Near the 12 Hz and 24 Hz frequencies, the average effective damping of eccentricity fluctuates, so the seal stability is poor. The negative effect of exciting forces increases, and the seal stability is improved when the eccentricity increases. When the phase difference between the excitation force and displacement changes, the seal stability decreases. The fundamental reason for rotor instability induced by steam flow excited vibration in seals is the sharp changes of phase difference caused by pressure fluctuations.

Keywords: ultra-supercritical unit, labyrinth seal, steam flow excited vibration, dynamic characteristics, phase-frequency analysis

Highlights

- *A new simulation method of rotor whirling was verified by experiments.*
- *Average effective damping and fluid working were effectively calculated.*
- *Seal stability was analysed using average effective damping and fluid working.*
- *The mechanism of rotor instability was revealed via phase-frequency characteristics.*

0 INTRODUCTION

The vibration in rotational machinery seriously affects operational safety. As the main factor inducing rotor instability, steam flow excited vibration is becoming increasingly significant in steam turbines, especially for supercritical units [1] and [2].

Steam flow excited vibration has attracted much attention since Alford proposed it, and the research methods to analyse steam flow excited vibration are different from the analysis of other characteristics [3]. Experimental measurements and the simplified Alford formula analysis were usually adopted at the beginning of the study. In the analysis of the seal's internal flow field, the sources for the steam flow excited vibration are the rotational motion and eccentricity of the rotor [4]. Therefore, scholars put forward theoretical calculation models of single-control volume, two-control volume, three-control volume, and multi-control volume to study the seal internal flow field [5]. Considering the shortcomings of the linear model, Muszynska and Bently [6] developed a non-linear Muszynska model by incorporating the fluid inertia force into the linear eight-parameter model, but its accuracy in large eccentric whirl motion is poor. Si et al. [7] calculated the exciting forces and dynamic characteristics of a seal via the oscillating fluid dynamics method. The three-dimensional exciting flow field with blades was calculated by the amplitude equation of a viscous oscillating flow field. Zhang et al. [8] pointed out that the work performed by the seal fluid was the main factor affecting the steam flow excited vibration. The application of computational fluid dynamics (CFD) provides a new strategy to study steam flow excited vibration. The static eccentricity model was used to analyse the manner in which exciting forces vary with eccentricity and rotational velocity [9] in the investigation of exciting forces. The influences of inlet prewhirl and the pressure ratio on exciting forces are studied through the improved static eccentricity model, also known as the relative rotational model [10]. In the field of seal-rotor dynamic characteristics, Li et al. [11] solved the seal dynamic characteristics by simplifying the dynamic coefficients formula. Duan et al. [12] used the bulk-flow integral flow model to analyse the seal dynamic characteristics with the change in rotational velocity. Xia et al. [13] validated the consistency between bulk-flow results and experimental results. In order to predict the influence of steam flow excited vibrations on rotor stability, researchers [14] to [16] established the multi-frequency rotor whirl model

*Corr. Author's Address: Guangdong Datang International Leizhou Power Generation Co., Ltd., Leizhou 524255, Guangdong Province, China, hongtao169@163.com

to analyse the dynamic coefficients of compressor rotors in the frequency domain. The rule governing the variation of effective damping with pressure ratio and prewhirl was obtained. The critical point for the rotor instability, namely the crossing frequency, is calculated. When the seal structure affecting the steam flow excited vibration was taken into account, the dynamic coefficients of bent seal teeth were simulated and solved. The results show that the bent seal teeth reduce the rotor stability. Sun et al. [17] and [18] used the single-frequency whirl model to analyse the dynamic characteristics of the tapered clearance seal, wherein the concept of whirl work was proposed to analyse the rotor stability.

In terms of research technology, scholars have proposed many effective calculation methods to improve the accuracy and timeliness of solving vibration. Meng et al. [19] improved the Riccati transfer matrix method by considering contact effects based on the framework of a traditional Riccati transfer matrix method. Peng et al. [20] proposed a synchronous vibration control method with a two-stage notch filter for the magnetically suspended rotor system, and the experimental results were used to confirm the effectiveness of the method. Ahmadi et al. [21] developed a meshless formulation to discretize the governing equations. The free vibration of two-directional functionally graded multiple nanobeam systems is studied. On this basis, the impact response of a nanobeam with a moving nanoparticle is investigated. The interaction between the nanoparticle and nanobeam was described by Lennard-Jones potential theory. The equations are discretized using the radial basis meshless method [22]. Na et al. [23] developed a dynamic coupling model for a hollow overhung rotor with external load excitation. Moreover, the Newmark-? numerical integration method was used to solve for the dynamic response of the overhung rotor under multiple excitation forces. Dong et al. [24] proposed an improved active disturbance rejection control to overcome poor error suppression performance and low control accuracy in the polishing robot-driven branch chain control system. Sun et al. [25] proposed a theoretical model for the forced vibration of time-varying elevator traction systems.

The research studies on steam flow excited vibration mainly focus on the analysis of exciting forces and dynamic coefficients. However, the mechanism of rotor instability induced by exciting forces and the relationship between the exciting forces and the rotor motion is not clear. In addition, most of the studies focus on gas turbines, compressors, and sub-critical steam turbines. However, the special operational and structural parameters of ultra-supercritical units make the steam flow excited vibration more prominent. Therefore, the multi-frequency whirl motion of large diameter rotors is achieved through user-defined functions (UDF) DEFINE_CG_MOTION and DEFINE_PROFILE. The rotor stability is analysed using the average effective damping and fluid work method. The mechanism of rotor instability induced by steam flow excited vibration is revealed through the phase-frequency characteristics of exciting forces and displacements. This mechanism provides a theoretical basis for the safe operation of ultra-supercritical steam turbines.

1 NUMERICAL MODEL AND METHODS

1.1 Computational Model

The full-cycle labyrinth seal model is established based on the second stage diaphragm seal in the super high-pressure cylinder of the 1000 MW steam turbine. As shown in Fig. 1, the leakage steam flows in the seal at the seal inlet, passes through the seal chamber and flows out through the outlet, forming turbulent flow inside the seal. The side near the inlet and the outlet of the seal is deformed by a mesh deformation. The specific structural parameters are shown in Table 1.

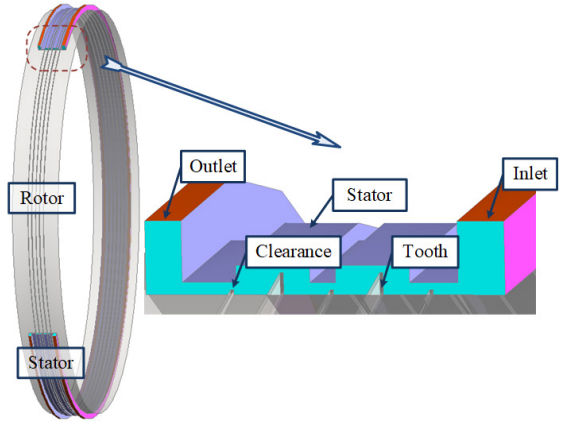

Fig. 1. *Model of labyrinth seal*

The unstructured grid is meshed by ANSYS ICEM. The transient flow field in the seal is simulated based on the pressure solver, in which the standard $k-\varepsilon$ turbulence model from the literature [26] and [27] is adopted. The flow inside the seal is close to isenthalpic flow, and flow velocity is high; the

compressible flow of actual steam and wall adiabatic boundary conditions are used.

The calculation errors of exciting forces are less than 0.05 % when the grid number is over 9.5 million. Therefore, a grid number between 9.5 and 11 million is selected to calculate the physical model.

Table 1. *Seal structural parameters*

Name	Axial length [mm]	Radial length [mm]
Inlet	8.4	452
Clearance	-	1.2
Stator	45.4	444.8
Cavity width	9.6/12.6	444.8
Tooth	0.4	440.8/443.6
Rotor	60	440
Deform	-	452
Outlet	6.2	452

1.2 Whirl Equation

The mesh deformation in Fluent is adopted to achieve field deformation, in which the user-defined function DEFINE_CG_MOTION is established to control the multi-frequency rotor whirl motion. Taking the Y-Z plane coordinate system as an example, the whirl equation is as follows:

$$\dot{z} = -e/12.5 \times \sum \Omega_m \times \cos\left(\Omega_m \times t\right), \tag{1}$$

$$\dot{y} = -e/12.5 \times \sum \Omega_m \times \sin\left(\Omega_m \times t\right). \tag{2}$$

In the equations above, e is the whirl radius of the rotor, $\dot{z}(t)$ and $\dot{y}(t)$ are the rotor centre velocities in the z and y directions, respectively, Ω is the whirl velocity, t is the time, and subscript m is the corresponding frequency of rotor whirl, which is 5, 10, and 10, …, 60 Hz.

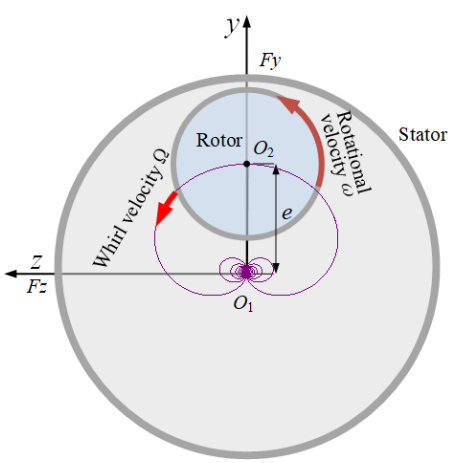

Fig. 2. *Rotor whirl motion*

Twelve frequency points (m = 12), including 5 Hz to 60 Hz frequencies, are selected to accurately identify the distribution of dynamic characteristics in the frequency domain. The rotor whirl motion is shown in Fig. 2.

The rotor diameter of the ultra-supercritical unit is 880 mm, so the maximum linear velocity of the rotor surface is about 139 m/s. In order to avoid generating negative volume grids, the calculation time step that consumes a significant amount of time needs to be about 10^{-6} seconds. The reference frame rotational coordinate system is established by DEFINE_PROFILE, which avoids negative volume grids and improves the calculation performance. The time step of the simulation is 10^{-4} s to ensure the accuracy of frequency recognition. The rotational motion of the motor is shown in Fig. 3. The specific transformation is as follows:

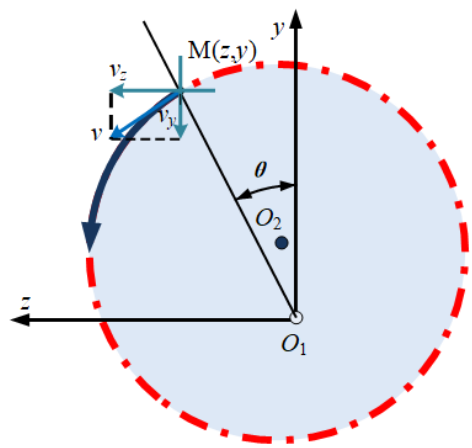

Fig. 3. *Rotor rotational motion*

There exists an assumed node M(z,y) on the surface of the eccentric rotor, such that the distance between node M and the coordinate origin O_1 is:

$$r = \sqrt{z^2 + y^2}. \tag{3}$$

The angle between the node M and the y-axis at time t is expressed as:

$$\theta = \arctan 2(z, y). \tag{4}$$

The linear velocities of M in the orthogonal direction are expressed as:

$$v_y = -\omega r \sin\theta, \tag{5}$$

$$v_z = -\omega r \cos\theta, \tag{6}$$

if $z>0$, $v'_y=-v_y$, if $z<0$, $v'_y=v_y$; similarly, if $y>0$, $v'_z=-v_z$, if $y<0$, $v'_z=v_z$. The rotational motion of the

rotor at any position can be obtained by traversing each node.

1.3 Solution of Dynamic Coefficients

The relationship between the steam flow exciting forces and the dynamic coefficients in the seal can be expressed by the following equation:

$$-\begin{bmatrix} F_z \\ F_y \end{bmatrix} = \begin{bmatrix} k_{zz} & k_{zy} \\ k_{yz} & k_{yy} \end{bmatrix} \begin{bmatrix} z \\ y \end{bmatrix} + \begin{bmatrix} c_{zz} & c_{zy} \\ c_{yz} & c_{yy} \end{bmatrix} \begin{bmatrix} \dot{z} \\ \dot{y} \end{bmatrix}, \quad (7)$$

where F_z and F_y are the component forces in z and y direction, [N]; k_{zz} and k_{yy} are the direct stiffness, [N/m]; k_{zy} and k_{yz} are the cross-coupling stiffness, [N/m]; c_{zz} and c_{yy} are the direct damping, [N·s/m]; c_{zy} and c_{yz} are the cross-coupling damping, [N·s/m]; z and y are the displacements in the z and y direction, [m].

When the whirl frequency is determined, the rotor centre motion can be expressed as:

$$\dot{z} = \Omega \times z, \quad (8)$$

$$\dot{y} = \Omega \times y. \quad (9)$$

Seal dynamic characteristics related to displacements can be obtained according to Eqs. (7) to (9).

$$-\begin{bmatrix} F_z \\ F_y \end{bmatrix} = \begin{bmatrix} k_{zz} + \Omega c_{zz} & k_{zy} + \Omega c_{zy} \\ k_{yz} + \Omega c_{yz} & k_{yy} + \Omega c_{yy} \end{bmatrix} \begin{bmatrix} z \\ y \end{bmatrix}. \quad (10)$$

The dynamic coefficient equations in the frequency domain are transformed through Fast Fourier transforms (FFT).

$$-\begin{bmatrix} \mathcal{F}(F_z) \\ \mathcal{F}(F_y) \end{bmatrix} = \begin{bmatrix} k_{zz} + \Omega c_{zz} i & k_{zy} + \Omega c_{zy} i \\ k_{yz} + \Omega c_{yz} i & k_{yy} + \Omega c_{yy} i \end{bmatrix} \begin{bmatrix} \mathcal{F}(z) \\ \mathcal{F}(y) \end{bmatrix}, \quad (11)$$

where $\mathcal{F}(F_z)$, $\mathcal{F}(F_y)$, $\mathcal{F}(z)$, and $\mathcal{F}(y)$ are complex numbers in the form of $a + bi$ after the execution of FFT.

According to the small perturbation theory of rotor dynamics, the dynamic characteristics are approximately invariant. They are frequency-dependent functions. Thus, the whirl equations in both positive and negative directions are established as follows.

$$-\begin{bmatrix} \mathcal{F}(F_{z1}) & \mathcal{F}(F_{z2}) \\ \mathcal{F}(F_{y1}) & \mathcal{F}(F_{y2}) \end{bmatrix} = \begin{bmatrix} k_{zz} + \Omega c_{zz} i & k_{zy} + \Omega c_{zy} i \\ k_{yz} + \Omega c_{yz} i & k_{yy} + \Omega c_{yy} i \end{bmatrix} \times \begin{bmatrix} \mathcal{F}(z_1) & \mathcal{F}(z_2) \\ \mathcal{F}(y_1) & \mathcal{F}(y_2) \end{bmatrix}. \quad (12)$$

Finally, the rotor dynamic coefficients can be calculated as follows:

$$k_{zz} + \Omega c_{zz} i = \frac{-\mathcal{F}(F_{z2})\mathcal{F}(y_1) - (-\mathcal{F}(F_{z1}))\mathcal{F}(y_2)}{\mathcal{F}(z_2)\mathcal{F}(y_1) - \mathcal{F}(z_1)\mathcal{F}(y_2)}, \quad (13)$$

$$k_{zy} + \Omega c_{zy} i = \frac{-\mathcal{F}(F_{z2})\mathcal{F}(z_1) - (-\mathcal{F}(F_{z1}))\mathcal{F}(z_2)}{\mathcal{F}(y_2)\mathcal{F}(z_1) - \mathcal{F}(y_1)\mathcal{F}(z_2)}, \quad (14)$$

$$k_{yz} + \Omega c_{yz} i = \frac{-\mathcal{F}(F_{y2})\mathcal{F}(y_1) - (-\mathcal{F}(F_{y1}))\mathcal{F}(y_2)}{\mathcal{F}(z_2)\mathcal{F}(y_1) - \mathcal{F}(z_1)\mathcal{F}(y_2)}, \quad (15)$$

$$k_{yy} + \Omega c_{yy} i = \frac{-\mathcal{F}(F_{y2})\mathcal{F}(z_1) - (-\mathcal{F}(F_{y1}))\mathcal{F}(z_2)}{\mathcal{F}(y_2)\mathcal{F}(z_1) - \mathcal{F}(y_1)\mathcal{F}(z_2)}. \quad (16)$$

2 CALCULATION AND ANALYSIS

2.1 Numerical Boundaries and Verification

A 1:2 steam flow excited vibration experiment was established to verify the turbulence model and the relevant boundary conditions. The stage is composed of 45 rotor blades and 45 stator blades. The steam parameters in a 1000 MW steam turbine are high, so the air is used as a working medium with the consideration of experimental safety. The air is driven by an asynchronous fan to flow through the rectifier section and enter the rotor-seal experiment section. The rotor rotational velocity is maintained around 3000 r/min by controlling the air volume. The experimental system of the steam flow excited vibration is as shown in the Fig. 4.

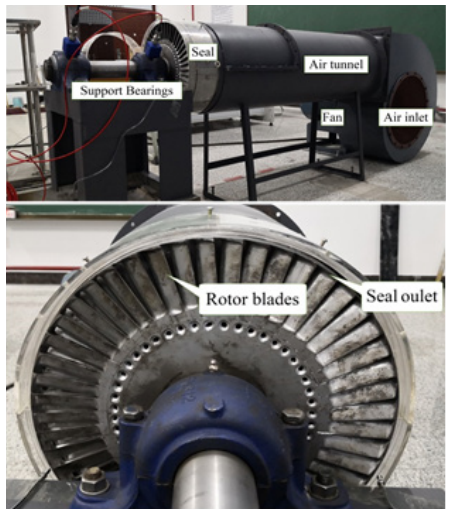

Fig. 4. *Experimental system of steam flow excited vibration*

The air pressure at the stator inlet is 3200 Pa, and the air temperature is 20 °C. Because the measurement

errors of vibration signal and exciting force are large, the variation of seal outlet pressure is measured by the pressure sensor, as shown in Fig. 5. Meanwhile, the numerical simulation has the same boundary.

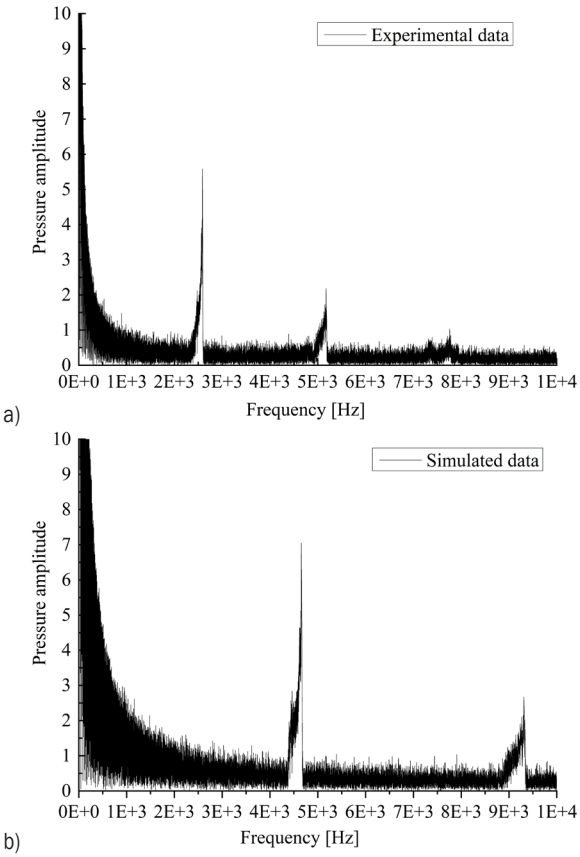

Fig. 5. *Pressure at seal outlet; a) experimental data, and b) simulation data*

The experimental rotor has 45 blades, so its pressure fluctuation frequency is 45 blades × 50 Hz. The actual turbine rotor has 90 moving blades, so its pressure fluctuation frequency is 90 blades × 50 Hz. However, there are some problems, such as air leakage in the experiment, so the final pressure amplitude in the experiment will be smaller than the simulation value. From the frequency of pressure fluctuations, there are disturbances in the operating frequency and second harmonic in both experimental and simulation results. In the experiment, there was even a small disturbance of triple frequency. However, in the simulation, there was no triple-frequency disturbance of pressure. This is because there were many simulated blades, and the excessively high frequency was not recognized. However, from the perspective of frequency amplitude, the simulation results can obtain significant pressure fluctuations and have a certain degree of reliability.

Furthermore, the boundary and steam parameters are set at the values they would have at 100 % turbine heat acceptance (THA), as shown in Table 2. Comparing the average direct stiffness with that of literature **[15]** and **[28]** as shown in Fig. 6, the seal dynamic coefficient calculated by Fluent has the same accuracy as computational fluid X (CFX), and they are close to the experimental value of Ertas. However, there are still errors between the simulation results and the experimental results. There are two reasons for this. The first reason is that there are errors in the measurement sensors of displacement and force used in the experiment, and the airtightness of the experimental seal is poor, resulting in a smaller force measurement. The second reason is that the experimental results are based on the first-order relationship between force and displacement. Therefore, there is a numerical deviation between the simulation results and the experimental results, and the changing trend is consistent.

Table 2. *Boundary properties and parameters*

Name	Properties	Parameters
Inlet	Pressure inlet	18.96 MPa, 544.2 °C
Clearance	Radial variation	Following rotor
Stator	Static	0 r/min
Cavity width	Radial variation	Following rotor
Tooth	Rotating	Following rotor
Rotor	Rotating	3000 r/min
Deform	Deformation	Following rotor
Outlet	Pressure outlet	18.03 MPa, 537.67 °C

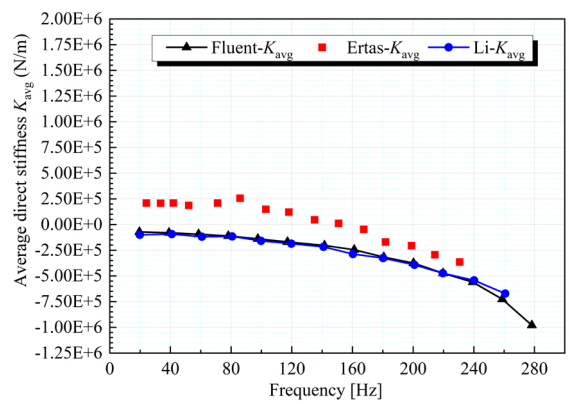

Fig. 6. *Average direct stiffness*

3 RESULTS AND DISCUSSION

The rotor dynamic characteristics with an initial eccentricity of 0.10 mm (8.33 % clearance) are obtained by FFT, as shown in Figs. 7 and 8. In the range of 5 Hz to 50 Hz, the cross-coupling stiffness k_{zy}, k_{yz}, and direct stiffness k_{zz} fluctuate, while the direct stiffness k_{yy} has a larger distribution range and its absolute value is larger. It indicates that the exciting forces have a greater impact on the vertical direction (y direction), and in particular, at frequencies greater than 55 Hz, the stiffness distribution has a large diffusion. The direct damping c_{zz} decreases gradually with the increase in frequency. c_{yy} decreases initially and then stabilizes, finally increasing at frequencies higher than 55 Hz. The cross-coupling damping decreases initially and then increases, finally stabilizing at frequencies higher than 15 Hz.

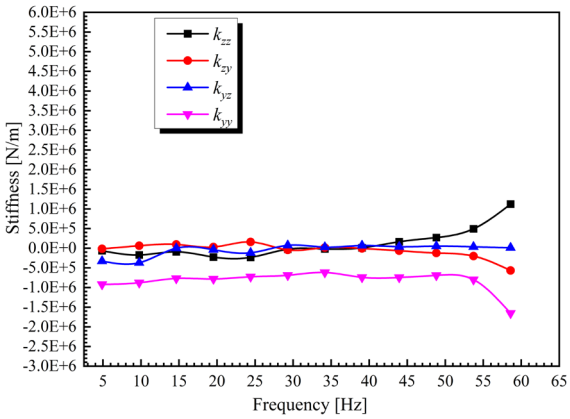

Fig. 7. *Direct stiffness and cross-coupling stiffness; e = 0.10 mm / 8.33 %*

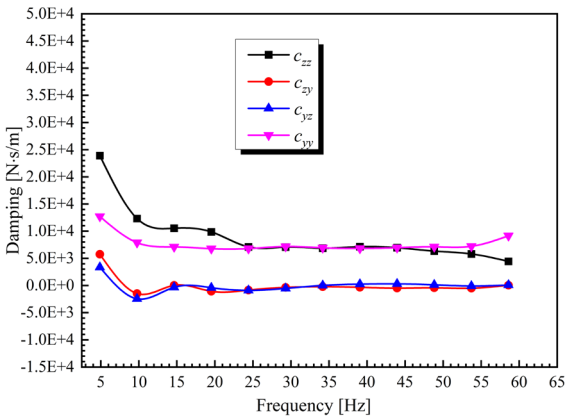

Fig. 8. *Direct damping and cross-coupling damping; e = 0.10 mm / 8.33 %*

Direct damping and cross-coupling stiffness have a great influence on the seal stability. It is expected that the seal stability is lower with an increase in frequency because the cross-coupling damping fluctuates, and the direct damping decreases with an increase in frequency.

The effective damping can be calculated using the cross-coupling stiffness and the direct damping, which predict the stability of the seal when it is affected by steam flow excited vibration. The larger the effective damping, the stronger the ability of the system to restrain steam flow excited vibration. If the effective damping is less than zero, the system is unstable. The definition of effective damping C_{E} is as follows:

$$C_{\mathrm{E}} = c_{zz} - k_{zy}/\Omega. \tag{17}$$

The non-linear variation of exciting forces in the seal makes the seal stability greatly susceptible to the influence of rotor eccentricity. Hence, the effective damping of three different initial eccentricities, 0.08 mm, 0.10 mm, and 0.12 mm (6.66 %, 8.33 %, and 10 % clearance) are given, as shown in Fig. 9.

The variation of effective damping is similar to the variation seen in direct damping–both of them decrease with an increase in frequency. Compared with the effective damping in literature [14] and [21], the distribution of effective damping in the high-frequency region is consistent, thus validating the reliability of the present results. We observe that the seal stability decreases with an increase in frequency. The effective damping eccentricity of 6.66 % is larger in the low-frequency range, while the other eccentricities at other frequencies are low. The effective damping of the eccentricity of 8.33 % fluctuates and decreases greatly near a frequency of 24 Hz, indicating that the seal stability is poor. Although some researchers pointed out that the dynamic coefficients under the small disturbance theory are independent of eccentricity, the eccentricity still has an effect on the dynamic characteristics at low whirl frequency in the steam flow excited vibration.

It is difficult to analyse the seal stability in the high-frequency range because the effective damping at the three eccentricities becomes similar with the increase in frequency. The steam in the seal will work (fluid work) on the rotor in the process of rotor whirl, and the ability of the rotor to absorb the fluid's work varies with the pressure fluctuation and rotor displacement. If the steam works positively on the rotor, the rotor absorbs energy that would intensify the rotor whirl. Otherwise, if the steam acts negatively on the rotor, the kinetic energy of the rotor would be decreased. Therefore, the rotor whirl is weakened, and

the stability is excellent. The definition of fluid work for a given frequency is as follows:

$$W_{\text{steam}} = -\int_0^T \left(F_z \dot{z} + F_y \dot{y}\right) \mathrm{d}t, \tag{18}$$

$$F_z = \frac{e}{12.5}\begin{pmatrix} k_{zz}\sin(\Omega t) - k_{zy}\cos(\Omega t) \\ +c_{zz}\Omega\cos(\Omega t) + c_{zy}\Omega\sin(\Omega t) \end{pmatrix}, \tag{19}$$

$$W_{\text{steam}} = \frac{e^2\pi}{12.5^2}\left(\left(k_{zy} - k_{yz}\right) - \Omega\left(c_{zz} + c_{yy}\right)\right), \tag{20}$$

$$C_{\text{EA}} = \left(k_{zy} - k_{yz}\right)/\Omega - \left(c_{zz} + c_{yy}\right). \tag{21}$$

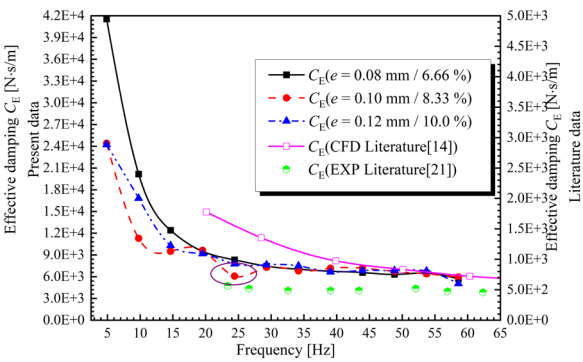

Fig. 9. *Effective damping*

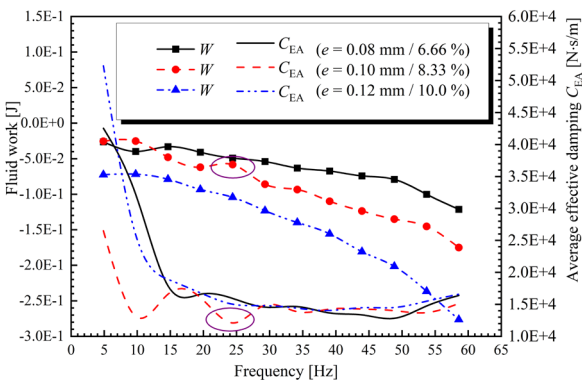

Fig. 10. *Steam exciting forces work*

As shown in Fig. 10, the fluid in the seal works negatively on the rotor, indicating that the rotor whirl is restrained. The greater the initial eccentricity, the greater the negative influence of the fluid action. In the analysis of the work done by the fluid, the work done by the fluid at a large eccentricity is higher than that at a small eccentricity in the low-frequency range; that is, the stability of the seal is better with large eccentricities. However, from effective damping, the stability of a seal with a low eccentricity is better in the low-frequency range. This is because of the quadratic relationship between the work done by the fluid and initial eccentricity, *e*. Therefore, the variation of fluid work is larger because of the influence of initial eccentricity, *e*. Furthermore, only the dynamic coefficients c_{zz} and k_{zy} are considered in effective damping, i.e., c_{yy} and k_{yz} are ignored. The observations above can be clearly understood from Eqs. (17) and (21). The average effective damping C_{EA} is calculated after eliminating the initial eccentricity e and whirl velocity Ω, wherein the effects of c_{zz}, k_{zy} and c_{yy}, k_{yz} are taken into account, as shown in Fig. 10. The variation of C_{EA} is similar to effective damping, with the fluid work and C_{EA} both fluctuating greatly at 24 Hz. The negative work performed by the fluid decreases. Therefore, the seal stability is poor.

$$C_{\text{EA}} = \left(k_{zy} - k_{yz}\right)/\Omega - \left(c_{zz} + c_{yy}\right). \tag{22}$$

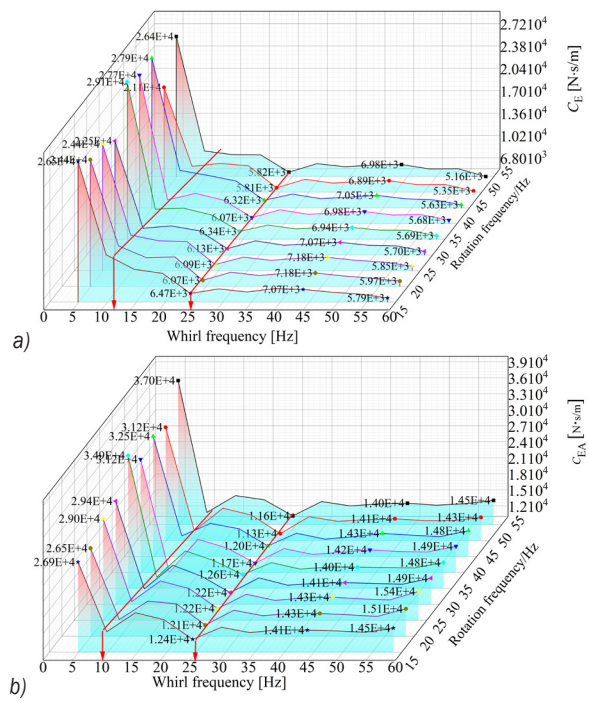

Fig. 11. *Seal damping at different rotational velocities; a) effective damping C_{EA}, and b) average effective damping C_{EA}*

The effective damping C_{E} and average effective damping C_{EA} at different rotational velocities are calculated, as shown in Fig. 11. Both of them decrease with the increase in frequency. The average effective damping C_{EA} fluctuates near the rotational frequency of 12 Hz; however, C_{E} does not exhibit such a variation clearly. Moreover, the average effective damping shows an upward trend at frequencies greater than 55 Hz. Considering the actual operation of the steam turbine, the rotational frequencies of 12 Hz and 24 Hz are close to 0.5 times the critical velocity of the

rotor or equal to it, respectively. Further, the velocity is far removed from that required for the resonance zone at frequencies greater than 55 Hz. Therefore, the seal stability will be poor near 12 Hz and 24 Hz and improved at values greater than 55 Hz. We conclude that the stability estimated by C_{EA} is more comprehensive.

The exciting forces and displacements were analysed through the vibration theory of damped systems to study the influence of steam flow excited vibration on the rotor motion. The complex numbers of the exciting forces and displacements in the frequency domain are as follows:

$$\mathcal{F}\left(F_z\right)=a_{Fz}+b_{Fz}i, \tag{23}$$

$$\mathcal{F}\left(F_y\right)=a_{Fy}+b_{Fy}i, \tag{24}$$

$$\mathcal{F}\left(z\right)=a_z+b_zi, \tag{25}$$

$$\mathcal{F}\left(y\right)=a_y+b_yi. \tag{26}$$

The direct phase difference and cross-coupling phase difference $\Delta\varphi_{zz}$, $\Delta\varphi_{yy}$, $\Delta\varphi_{zy}$, and $\Delta\varphi_{yz}$ between the exciting forces and displacements in the z and y directions can be expressed as follows:

$$\Delta\varphi_{zz}=\arctan\left(\frac{b_{Fz}}{a_{Fz}}\right)-\arctan\left(\frac{b_z}{a_z}\right), \tag{27}$$

$$\Delta\varphi_{yy}=\arctan\left(\frac{b_{Fy}}{a_{Fy}}\right)-\arctan\left(\frac{b_y}{a_y}\right), \tag{28}$$

$$\Delta\varphi_{zy}=\arctan\left(\frac{b_{Fz}}{a_{Fz}}\right)-\arctan\left(\frac{b_y}{a_y}\right), \tag{29}$$

$$\Delta\varphi_{yz}=\arctan\left(\frac{b_{Fy}}{a_{Fy}}\right)-\arctan\left(\frac{b_z}{a_z}\right). \tag{30}$$

The relationships between the exciting forces and displacements corresponding to the phase difference are as shown in Table 3.

Table 3. *Relationship between forces and displacements*

$\Delta\varphi$	Relative direction/relationship	Stability
0°or 360°	Forward direction / Coincidence	Poor
0° ~ 90°	Forward direction / Phase advance	Poor
$\Delta\varphi$ = 90°	Forward direction / Phase orthogonality	Critical
90° ~ 180°	Inverse direction / Phase advance	Good
$\Delta\varphi$ = 180°	Inverse direction / Coincidence	Best
180° < $\Delta\varphi$ < 270°	Inverse direction / Phase lag	Good
$\Delta\varphi$ = 270°	Inverse direction / Phase orthogonality	Critical
270°< $\Delta\varphi$ < 360°	Forward direction / Phase lag	Poor
$\Delta\varphi$ fluctuates	Phase lag to advance	Worst

Fig. 12 shows the phase differences between the exciting forces and displacements at an 8.33 % eccentricity (initial eccentricity is 0.10 mm). The phase difference $\Delta\varphi_{yy}$ is always between 0° and 90°, implying that the exciting force F_y is in the same direction as displacement y and that the exciting force is ahead of displacement, i.e., they are not conducive to the seal stability. Further, the phase difference $\Delta\varphi_{zz}$ in the range of 0 Hz to 40 Hz is between 0° and 90°, and $\Delta\varphi_{zz}$ in the range of 40 Hz to 60 Hz is between 90° and 180°. Hence, the exciting force F_z and displacement z contain the inverse component, which is beneficial to seal stability. The phase difference $\Delta\varphi_{zy}$ is between 270° and 360°. Therefore, the exciting force F_y and displacement z are in the same direction. The phase difference $\Delta\varphi_{zy}$ is between 90° and 180°, which is beneficial in restraining rotor motion. Based on the phase analysis of the exciting forces in the direct and cross-coupling directions, it can be seen that the exciting force F_y is the forward component with displacement y and z. However, the exciting force F_z is the inverse component with displacement y and z. From the perspective of the work done by the fluid, it is primarily the exciting force F_y that performs positive work on the rotor, while the exciting force F_z mainly results in negative work on the rotor.

The phase differences $\Delta\varphi_{yy}$ and $\Delta\varphi_{zy}$ gradually increase with an increase in frequency, while the phase difference $\Delta\varphi_{zz}$ first decreases and then increases. On the other hand, the phase difference $\Delta\varphi_{zz}$ fluctuates, but with an increase of 20° at 24 Hz. The $\Delta\varphi_{yz}$ and $\Delta\varphi_{zz}$ also fluctuate at 24 Hz, but the fluctuation trends in the opposite manner. The increase of positive work done by the fluid by the exciting force Fy results in the decrease of total negative fluid work. Therefore, the average effective damping C_{EA} and fluid work W fluctuate near 24 Hz (Figs. 9 and 10), and the seal stability decreases. Similarly, the stability fluctuates between 9.8 Hz and 15 Hz due to the change of $\Delta\varphi_{zz}$ and $\Delta\varphi_{yz}$, wherein $\Delta\varphi_{zz}$ increases from 65° to 83° and $\Delta\varphi_{yz}$ is decreased by 18°.

Steam flow exciting forces arise primarily due to the uneven distribution of pressure when the rotor is eccentric; however, the effect of pressure fluctuations caused by the rotor whirl on the exciting forces is not clear. Fig. 13 shows the distribution of the exciting force and the pressure on the rotor surface at 0.2 s (rotor eccentricity on the y-axis is 0.1 mm). Because of the high-pressure parameters in the supercritical unit, it is difficult to analyse the absolute pressure. The axial average exciting forces and pressure amplitudes of nodes at different circumferential angles are given.

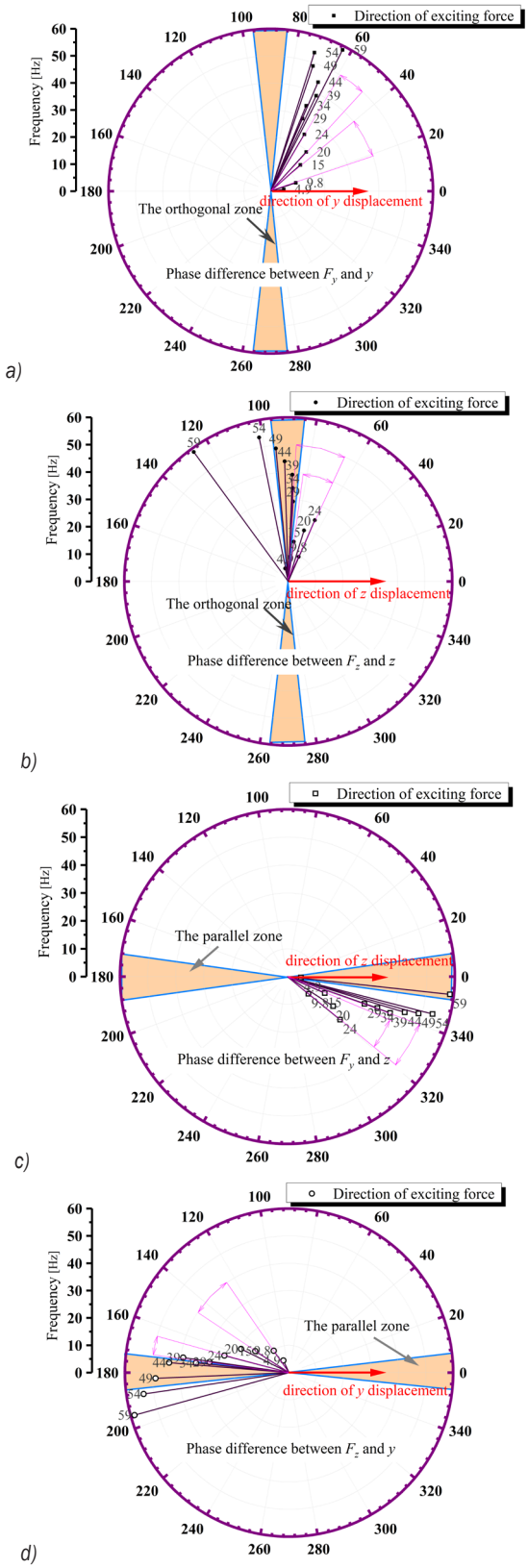

Fig. 12. *Phase frequency distribution of exciting forces and displacements at a) $\Delta\varphi_{yy}$, b) $\Delta\varphi_{zz}$, c) $\Delta\varphi_{yz}$, and d) $\Delta\varphi_{zy}$*

The expression of axial average exciting force and pressure amplitudes are as follows:

$$F_i = \frac{1}{n}\sum_{j=1}^{n} F_{ij}, \tag{31}$$

$$P_i = \frac{1}{n}\sum_{j=1}^{n} P_{ij}, \tag{32}$$

where n is the node number along the x direction in an arc angle $\Delta\theta_i$, i is the arcs number in a circle, and $i=18$.

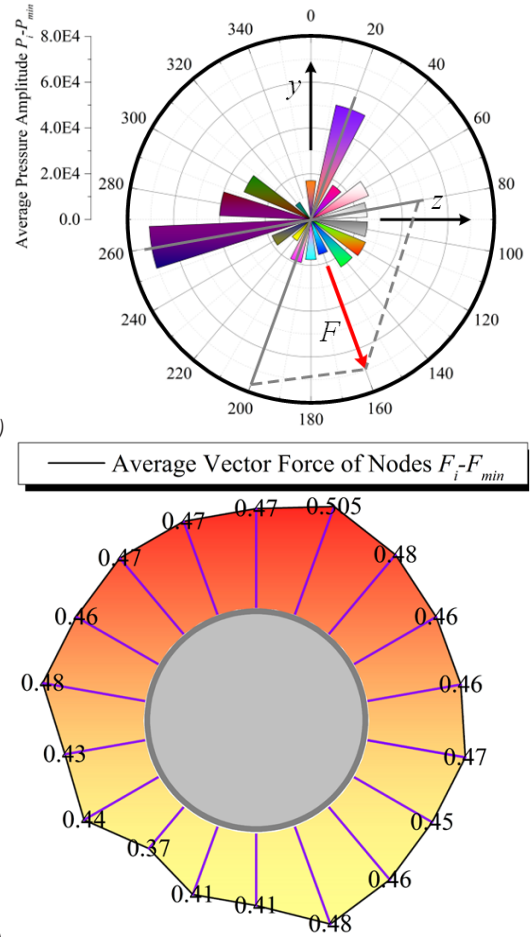

Fig. 13. *Exciting force and pressure amplitudes on the rotor at t = 0.2 s; a) amplitude of exciting force, and b) amplitude of average pressure*

It can be seen from Fig. 13a that the exciting force at a small clearance is larger when the rotor is upwardly eccentric, resulting in the resultant force pointing in the direction of the negative y-axis. At the same time, the steam is compressed in the second quadrant zone because of the influence of rotor whirl, and the pressure is higher; therefore, the exciting force

on the upper left side of the rotor is higher than that on the upper right side; this eventually makes the exciting force point to the fourth quadrant. In combination with Fig. 13b, we observe that the pressure fluctuation appears at circumferential positions of 20° and 260°, and the pressure amplitude is higher than at other locations. The resultant force on the rotor is also in the same direction as Fig. 13a. Therefore, the pressure distribution in the eccentric rotor seal system is always uneven; however, the main reason for the prominent steam flow exciting force is the amplitude of the high pressure, and the vector direction of the pressure fluctuation is consistent with that of the exciting force.

4 CONCLUSIONS

The multi-frequency whirl model for the ultra-supercritical turbine seal is established through a user-defined function and mesh deformation. The dynamic characteristics with steam flow excited vibration in the seal are solved. The seal stability in the frequency domain is analysed using the average effective damping and fluid work method. The mechanism of rotor instability induced by steam flow excited vibration is revealed based on the phase-frequency characteristics of the exciting forces and displacements. The specific conclusions are as follows:

1. The whirl motion of the large diameter rotor is established based on the user-defined function DEFINE_CG_MOTION, and the rotational motion at any position is obtained by the function DEFINE_PROFILE, which makes the mesh deformation effective. The negative volume grids in the seal model caused by excessive linear velocity are avoided.
2. The cross-coupling stiffness k_{zy}, k_{yz}, and direct stiffness kzz fluctuate in the range of 5 Hz to 50 Hz. The direct stiffness kyy has a large distribution range. The direct damping c_{zz} decreases with the increase of frequency, and the c_{yy} decreases initially and then stabilizes, finally increasing over 55 Hz. The cross-coupling damping decreases initially and then increases, finally stabilizing over 15 Hz. The seal stability is low with an increase in frequency.
3. The average effective damping take the effects of c_{zz}, k_{zy} and c_{yy}, k_{yz} into account, which is more comprehensive in prediction of seal stability. The effective damping decreases gradually with the increase in frequency, and the seal stability decreases. The average effective damping and fluid work fluctuates around 12 Hz and 24 Hz, which shows an upward trend over 55 Hz. The negative fluid work decreases, and the stability of the seal is poor. The greater the initial eccentricity, the more negative work the fluid performs.
4. The fundamental reason for rotor instability induced by steam flow excited vibration in the seal is that the phase difference between the exciting forces and displacements changes sharply. The exciting force F_y acts in the forward direction with displacements y and z, but the F_z acts in the inverse direction with displacements y and z. The exciting force is that F_y primarily performs positive work on the rotor, while F_z mainly performs negative work on the rotor.
5. The phase differences $\Delta\varphi_{yy}$ and $\Delta\varphi_{zy}$ gradually increase with an increase in frequency, which is always between 0° and 90°. The phase difference $\Delta\varphi_{zz}$ first decreases and then increases. The phase differences $\Delta\varphi_{zz}$ and $\Delta\varphi_{yz}$ fluctuate at 12 Hz and 24 Hz, and the increased range can be up to 20°, reducing the stability of the seal.

5 ACKNOWLEDGEMENTS

This work was supported by the Guangdong Datang International Leizhou Power Generation Co., Ltd. (CDTHT20230042372).

6 NOMENCLATURES

e	whirl radius of rotor, [m]
$\dot{z}(t)$	velocity in the z direction, [m/s]
$\dot{y}(t)$	velocity in the y direction, [m/s]
Ω	whirl velocity, [rad/s]
ω	rotational velocity, [rad/s]
t	time, [s]
F	steam exciting force, [N]
k	stiffness, [N/s]
c	damping, [N·s/m]
C_{E}	effective damping, [N·s/m]
C_{EA}	average effective damping, [N·s/m]
$z(t)$	displacement in the z direction, [m]
$y(t)$	displacement in the y direction, [m]
W	fluid work, [J]
n	nodes number
$\Delta\theta_i$	arc angle, [°]
$\Delta\varphi$	phase difference, [°]

Subscripts

z	z-direction in cartesian coordinates
y	y-direction in cartesian coordinates
m	whirl velocities
zz	From z to z-direction in cartesian coordinates

yy From *y* to *y*-direction in cartesian coordinates
zy From *z* to *y*-direction in cartesian coordinates
yz From *y* to *z*-direction in cartesian coordinates
1 Forward whirl motion
2 Backward whirl motion
i Arcs number

7 REFERENCES

[1] Yonezawa, K., Ogawa, R., Ogi, K., Takino, T., Tsujimoto, Y., Endo, T., Tezuka, K., Morita, R., Inada, F. (2012). Flow-induced vibration of a steam control valve. *Journal of Fluids and Structures*, vol. 35, p. 76-88, **DOI:10.1016/j.jfluidstructs.2012.06.003**.

[2] Jia, X., Zheng, Q., Jiang, Y. Zhang, H. (2019). Leakage and rotordynamic performance of T type labyrinth seal. *Aerospace Science and Technology*, 2019, vol. 88, p. 22-31, **DOI:10.1016/j.ast.2019.02.043**.

[3] Vance, J.M., Laudadio, F.J. (1984). Experimental measurement of Alford's force in axial-flow turbomachinery. *Journal of Engineering for Gas Turbines & Power*, vol. 106, no. 3, p. 585-590, **DOI:10.1115/1.3239610**.

[4] Rhode, D.L., Hensel, S.J., Guidry, M.J. (1993). Three-dimensional computations of rotordynamic force distributions in a labyrinth seal. *Tribology Transactions*, vol. 36, no. 3, p.461-469, **DOI:10.1080/10402009308983184**.

[5] Zahorulko, A.V., Lee, Y.B. (2021). Computational analysis for scallop seals with sickle grooves, part II: Rotordynamic characteristics. *Mechanical Systems and Signal Processing*, vo. 147, 107154, **DOI:10.1016/j.ymssp.2020.107154**.

[6] Muszynska, A., Bently, D.E. (1990). Frequency-swept rotating input perturbation techniques and identification of the fluid force models in rotor/bearing/seal systems and fluid handling machines. *Journal of Sound & Vibration*, vol. 143, no. 1, p. 103-124, **DOI:10.1016/0022-460X(90)90571-G**.

[7] Si, H., Cao, L., Li, P., Chen, D. (2021). Steam flow excited vibration and dynamic characteristics of seal in different rotor whirling motion. *Tribology International*, vol. 160, 107029, **DOI:10.1016/j.triboint.2021.107029**.

[8] Zhang, W., Wu, K., Gu, C., Tina, H., Zhang, X., Li, C. (2021). Swirl brakes optimization for rotordynamic performance improvement of labyrinth seals using computational fluid dynamics method. *Tribology International*, vol. 159, 106990, **DOI:10.1016/j.triboint.2021.106990**.

[9] Ding, X.J., Yang, Y.L., Chen, W., Huang, S.H., Zheng, C.G. (2006). Calculation method of efficiency factor in Alford's force. *Proceedings of the Institution of Mechanical Engineers, Part A: Journal of Power and Energy*, vol. 220, no. 2, p. 169-177, **DOI:10.1243/095765006X75983**.

[10] Wu, T., San Andrés, I. (2019). Gas labyrinth seals: On the effect of clearance and operating conditions on wall friction factors?A CFD investigation. *Tribology International*, vol. 131, p. 363-376, **DOI:10.1016/j.triboint.2018.10.046**.

[11] Li, Q., Liu, S.L., Zheng, S.Y., Sun, T.M. (2009). Numerical calculation of nonlinear dynamic characteristics for labyrinth seals. *Zhejiang Daxue Xuebao (Gongxue Ban)/Journal of Zhejiang University (Engineering Science)*, vol. 43, no. 3, p. 500-504, **DOI:10.3785/j.issn.1008-973X.2009.03.020**. (in Chinese)

[12] Duan, W., Chu, F., Kim, C.-H., Lee, Y.-B. (2007). A bulk-flow analysis of static and dynamic characteristics of floating ring seals. *Tribology International*, vol. 40, no. 3, p. 470-478, **DOI:10.1016/j.triboint.2006.04.010**.

[13] Xia, P., Liu, Z., Yu, Z., Zhao, J. (2018). A transient bulk flow model with circular whirl motion for rotordynamic coefficients of annular seals. *Chinese Journal of Aeronautics*, vol. 31, no. 5, p. 1085-1094, **DOI:10.1016/j.cja.2018.02.011**.

[14] Li, Z.G., Li, J., Yan, X. (2013). Multiple frequencies elliptical whirling orbit model and transient RANS solution approach to rotordynamic coefficients of annual gas seals prediction. *Journal of Vibration & Acoustics*, vol. 135, no. 3, 031005, **DOI:10.1115/1.4023143**.

[15] Li, Z, Li, J., Feng, Z.P. (2016). Comparisons of rotordynamic characteristics predictions for annular gas seals using the transient computational fluid dynamic method based on different single-frequency and multifrequency rotor whirling models. *Journal of Tribology*, vol. 136, no. 1, 011701, **DOI:10.1115/1.4030807**.

[16] Yan, X.,He, K., Li, J., Feng, Z. (2012). Rotordynamic performance prediction for surface-roughened seal using transient computational fluid dynamics and elliptical orbit model. *Proceedings of the Institution of Mechanical Engineers, Part A: Journal of Power & Energy*, vol. 226, no. 8, p.975-988, **DOI:10.1177/0957650912460358**.

[17] Sun, D., Wang, S., Xiao, Z., Meng, J., Wang, X., Zheng, T. (2015). Measurement versus predictions of rotordynamic coefficients of seal with swirl brakes. *Mechanism and Machine Theory*, vol. 94, p. 188-199, **DOI:10.1016/j.mechmachtheory.2015.08.009**.

[18] Sun, D., Li, S.Y., Xiao, Z.H., Meng J.G., Hu Y., Yu X.D. (2018). Rotordynamic characteristics analysis and suppression vibration mechanism of taper clearance hole-pattern damper seal. *Journal of Aerospace Power*, vol. 33, no. 7, p. 1544-1552, **DOI:10.13224/j.cnki.jasp.2018.07.002**. (in Chinese)

[19] Meng, C., Su, M., Wang, S. (2013). An investigation on dynamic characteristics of a gas turbine rotor using an improved transfer matrix method. *Journal of Engineering for Gas Turbines and Power*, vol. 135, no. 12, 122505, **DOI:10.1115/1.4025234**.

[20] Peng, C., Zhu, M., Wang, K., Ren, Y., Deng, Z. (2020). A two-stage synchronous vibration control for magnetically suspended rotor system in the full speed range. *IEEE Transactions on Industrial Electronics*, vol. 67, no. 1, p. 480-489, **DOI:10.1109/TIE.2018.2890498**.

[21] Ahmadi, I., Davarpanah, M., Sladek, J., Moradi, M.N. (2024). A size-dependent meshless model for free vibration analysis of 2D-functionally graded multiple nanobeam system. *Journal of Brazilian Society of Mechanical Science and Engineering*, vol. 46, 11, **DOI:10.1007/s40430-023-04580-5**.

[22] Ahmadi, I., Moradi, M.N., Panah, M.D. (2024). Dynamic response analysis of nanoparticle-nanobeam impact using nonlocal theory and meshless method. *Structural Engineering and Mechanics*, vol. 25, no. 2, 89, op. 135-153, **DOI:10.12989/sem.2024.89.2.135**.

[23] Na, R., Jia, K., Miao, S., Zhang, W., & Zhang, Q. (2023). Analysis of the dynamic characteristics of a gear-rotor-bearing

system with external excitation. *Strojniški vestnik - Journal of Mechanical Engineering*, vol. 69, no. (1-2), p. 17-31, **DOI:10.5545/sv-jme.2022.427**.

[24] Dong, K., Li, J., Lv, M., Li, X., Gu, W., & Cheng, G. (2023). Active disturbance rejection control algorithm for the driven branch chain of a polishing robot. *Strojniški vestnik - Journal of Mechanical Engineering*, vol. 69, no. (11-12), p. 509-521, **DOI:10.5545/sv-jme.2023.680**.

[25] Sun, J., Xu, P., Chen, M., & Xue, J. (2024). Forced Vibration of Time-Varying Elevator Traction System. *Strojniški vestnik - Journal of Mechanical Engineering*, vol. 70, no. (3-4), p. 170-180, **DOI:10.5545/sv-jme.2023.852**.

[26] Cao, L.H., Si, H.Y., Li, P., Li, Y. (2018). Study on the multi-factors influence on rotor dynamic characteristics and stability prediction. *Proceedings of the CSEE*, vol. 38, no. 3, p. 823-831, **DOI:10.13334/j.0258-8013.pcsee.170108**. (in Chinese)

[27] Chen, Y., Li, Z., Li, J., Yan, X. (2020). Effects of tooth bending damage on the leakage performance and rotordynamic coefficients of labyrinth seals. *Chinese Journal of Aeronautics*, vol. 33, no. 4, p. 1206-1217, **DOI:10.1016/j.cja.2019.12.004**.

[28] Ertas, B.H., Delgado, A., Vannini, G. (2012). Rotordynamic force coefficients for three types of annular gas seals with inlet preswirl and high differential pressure ratio. *Journal of Engineering for Gas Turbines and Power*, vol. 134, no. 4, 042503, **DOI:10.1115/1.4004537**.